Int J Thermophys (2009) 30:1649–1670
DOI 10.1007/s10765-009-0656-5

Heat Transfer in a Micropolar Fluid along a Non-linear Stretching Sheet with a Temperature-Dependent Viscosity and Variable Surface Temperature

Mohammad M. Rahman · M. A. Rahman · M. A. Samad · M. S. Alam

Received: 13 April 2009 / Accepted: 16 September 2009 / Published online: 8 October 2009

Abstract In this paper, heat transfer characteristics of a two-dimensional steady hydromagnetic natural convection flow of a micropolar fluid passed a non-linear stretching sheet taking into account the effects of a temperature-dependent viscosity and variable wall temperature are studied numerically for local similarity solutions by applying the Nachtsheim-Swigert iteration method. The results corresponding to the dimensionless temperature profiles and the local rate of heat transfer are displayed graphically for important material parameters. The results show that in modeling the thermal boundary layer flow with a temperature-dependent viscosity, consideration of the Prandtl number as a constant within the boundary layer produces unrealistic results and therefore it must be treated as a variable rather than a constant within the boundary layer. The results also show that the local rate of heat transfer strongly depends on the non-linear stretching index and temperature index.

Keywords Heat generation or absorption · Micropolar fluid · Non-linear stretching sheet · Variable viscosity · Variable wall temperature

M. M. Rahman (✉)
Department of Mathematics and Statistics, College of Science, Sultan Qaboos University, P.O. Box 36, P.C. 123 Al-Khod, Muscat, Sultanate of Oman
e-mail: mansurdu@yahoo.com

M. A. Rahman
Department of Mathematics, National University, Gazipur 1704, Bangladesh

M. A. Samad
Department of Mathematics, University of Dhaka, Dhaka 1000, Bangladesh

M. S. Alam
Department of Mathematics, Dhaka University of Engineering and Technology, Gazipur 1700, Bangladesh

List of Symbols

Variables

A	Constant
B	Constant
B_0	Magnetic induction
c	Stretching coefficient
c_p	Specific heat due to constant pressure
Ec	Eckert number
F_w	Dimensionless suction/injection velocity
f	Dimensionless stream function
Gr_x	Local Grashof number
g_0	Acceleration due to gravity
g	Dimensionless microrotation
j	Micro-inertia per unit mass
M	Local magnetic field parameter
m	Stretching index
N	Microrotation component normal to the xy-plane
Nu_x	Local Nusselt number
Pr_v	Variable Prandtl number
Pr_∞	Ambient Prandtl number
p	Temperature index
Q	Local heat source (or sink) parameter
Q_0	Heat generation/absorption coefficient
Re_x	Local Reynolds number
S	Coefficient of vortex viscosity
s	Microrotation parameter
T_∞	Temperature of the fluid within the boundary layer
T_r	Reference temperature
T_w	Temperature at the surface of the plate
T_∞	Temperature of the ambient fluid
u	The x-component of the velocity field
v	The y-component of the velocity field
$v_0(x)$	Suction/injection velocity
x	Axis in direction along the surface
y	Axis in direction normal to the surface

Greek

β	Volumetric coefficient of thermal expansion
γ	Richardson parameter
$\gamma*$	Constant
ρ	Fluid density
ρ_∞	Density of the ambient fluid
μ	Coefficient of dynamic viscosity
μ_∞	Coefficient of dynamic viscosity of the ambient fluid
υ	Coefficient of kinematic viscosity

υ_∞ Coefficient of kinematic viscosity of the ambient fluid
υ_s Spin-gradient viscosity
σ' Electrical conductivity of the fluid
ψ Stream function
ξ Micro-inertia density parameter
η Similarity variable
θ Dimensionless temperature
θ_r Variable viscosity parameter
k Thermal conductivity of fluid
Δ Vortex viscosity parameter

Subscripts

w Surface conditions
∞ Conditions far away from the surface

Superscript

$'$ Differentiation with respect to η

1 Introduction

The study of boundary layer flow over a moving continuous solid surface is important as it occurs in several engineering processes, for example, heat-treated materials travelling between a feed roll and a wind-up roll or materials manufactured by extrusion, glass-fiber and paper production, crystal growing, cooling of metallic sheets or electronic chips, etc. In these cases, the final product of desired characteristics depends on the rate of cooling in the process and the process of stretching. The dynamics of the boundary layer flow over a moving continuous solid surface originated from the pioneering work of Sakiadis [1] and have become a popular area of research due to its many engineering and physical applications as mentioned above. Since then, various aspects of the problem have been investigated by many authors. Erickson et al. [2] extended the problem of Sakiadis [1] considering wall suction at the moving surface to investigate its effects on the heat and mass transfer flow. Tsou et al. [3] studied flow and heat transfer in the boundary layer on a continuous moving surface while Gupta and Gupta [4] worked on the same problem in an extended view for a linearly moving surface. Chakrabarti and Gupta [5], Chiam [6], and Chandran et al. [7] have presented solutions for the flow and heat transfer of electrically conducting fluids over a stretched surface in the presence of a magnetic field. Vajravelu and Hadjinicalaou [8] have studied hydrodynamic convective flow along a stretching surface with uniform free stream in the presence of frictional heating and internal heat generation or absorption. Chen and Char [9] have investigated the effects of suction and injection on a stretched surface considering variable wall heat flux. Ali [10] investigated the effects of suction or injection on the thermal boundary layer flow considering a power-law stretched surface. Chen [11] studied the effects of a magnetic field and suction (or injection) on convective heat transfer flow of non-Newtonian power-law fluids passed a power-law

stretched sheet with surface heat flux. Cortell [12–14] studied heat transfer characteristics of Newtonian fluids over a non-linearly stretching sheet considering various flow conditions.

The microfluids are those which contain micro-constituents and can undergo rotation. These fluids are used in analyzing exotic lubricants, the flow of colloidal suspensions, paints, liquid crystals, animal blood, fluid flowing in brain, turbulent shear flows, and body fluids both mathematically and industrially. Since the early studies of Eringen [15,16] many researchers have reported results on micropolar fluids (see [17–23] and the references therein). Hossain and Chaudhury [24] have analyzed mixed convection flow of a micropolar fluid over an isothermal plate with a variable spin gradient viscosity. Rees and Pop [25] have studied free convection boundary layer flow of micropolar fluids along a vertical plate. Rahman and Sattar [26] studied magnetohydrodynamic convective flow of a micropolar fluid past a continuously moving vertical porous plate in the presence of heat generation or absorption. Rahman and Sattar [27] further studied their previous problem for unsteady flows with time dependent suction in the presence of radiation. Rahman and Sultana [28] studied radiative heat transfer flow of a micropolar fluid with variable heat flux in a porous medium. Rahman [29] studied convective flows of micropolar fluids from radiative isothermal porous surfaces with viscous dissipation and Joule heating. Very recently Rahman et al. [30] studied thermo-micropolar fluid flow along a vertical permeable plate with uniform surface heat flux in the presence of heat generation.

To date, most studies on boundary layers have given priority to the effect of constant viscosity. But the fluid viscosity changes with temperature. Pop et al. [31] studied the effect of variable viscosity on flow and heat transfer to a continuous moving flat plate. Elbashbeshy and Bazid [32] studied the effect of a temperature-dependent viscosity on heat transfer over a continuous moving surface. Abel et al. [33] studied visco-elastic fluid flow and heat transfer over a stretching sheet with variable viscosity. Ali [34] studied the effect of variable viscosity on mixed convection heat transfer along a vertical moving surface. Pantokratoras [35,36] studied the effects of variable viscosity on the laminar heat transfer flow of Newtonian fluids along a vertical/flat plate for various flow conditions. Mukhopadhyay [37] studied the effects of variable viscosity on the MHD boundary layer flow over a heated stretching surface. Alam et al. [38] studied transient magnetohydrodynamic free convective heat and mass transfer flow with thermophoresis past a radiative inclined permeable plate in the presence of a variable chemical reaction and temperature-dependent viscosity. Very recently Rahman and Salahuddin [39] have studied effects of a variable electric conductivity and temperature-dependent viscosity on magnetohydrodynamic heat and mass transfer flow along a radiative isothermal inclined surface with internal heat generation. All of the afore-mentioned research studies of variable viscosity are related to Newtonian fluids over a vertical (or flat) plate or along a linear stretching sheet.

Mohammadein and Gorla [40] studied the flow of micropolar fluids bounded by a stretching sheet with a prescribed wall heat flux, viscous dissipation, and internal heat generation. Desseaux and Kelson [41] studied the flow of a micropolar fluid bounded by a linearly stretching sheet while Bhargava et al. [42] studied the same flow over a non-linear stretching sheet. Hayat et al. [43] studied mixed convection flow of a micropolar fluid along a non-linear impermeable stretching sheet. However,

in their analysis the fluid viscosity as well as the surface temperature remain constant. To the best of our knowledge, heat transfer in hydromagnetic micropolar fluid flow considering a temperature-dependent viscosity and variable surface temperature in the presence of a heat source (or sink) over a non-linearly permeable stretching sheet remains unexplored.

Therefore, the objective of the present paper is to study the heat transfer characteristics of hydromagnetic micropolar fluid flow along a non-linear permeable stretched sheet taking into account a temperature-dependent viscosity with the non-linear variation of the surface temperature. The governing equations are reduced to non-linear ordinary differential equations which are solved by using the shooting method and the results are discussed from the physical point of view.

2 Mathematical Formulations

Let us consider a steady, laminar, and two-dimensional flow of a viscous incompressible micropolar fluid of temperature T_∞ past a non-linear stretching sheet whose temperature varies as $T_w = T_\infty + Ax^p$, where A is a dimensional constant and p is an exponent over a permeable surface coinciding with the plane $y = 0$, the flow being confined to $y > 0$. Two equal and opposite forces are introduced along the x-axis so that the surface is stretched keeping the origin fixed. The origin is located at the slit through which the sheet is drawn through the fluid medium, the x-axis is chosen along the sheet, and the y-axis is taken normal to it. The physical regime is illustrated in Fig. 1. This continuous sheet is assumed to move with a velocity according to the power law form, $u = cx^m$ where c is a dimensional constant known as the stretching rate and m is an arbitrary positive constant (i.e., not necessarily an integer) known as the stretching index. A magnetic field of uniform strength B_0 is applied in the y-direction, i.e., normal to the flow direction. There is a suction (or) injection velocity $v_0(x)$ normal to the sheet. It is to be mentioned that the porosity of the sheet, i.e., suction hole size is taken to be constant.

With the usual boundary layer and Boussinesq approximation, the governing equations of the problem are governed by (see [25]–[26])

$$\frac{\partial u}{\partial x} + \frac{\partial v}{\partial y} = 0, \tag{1}$$

$$u\frac{\partial u}{\partial x} + v\frac{\partial u}{\partial y} = \frac{1}{\rho_\infty}\frac{\partial}{\partial y}\left[(\mu + S)\frac{\partial u}{\partial y}\right] + \frac{S}{\rho_\infty}\frac{\partial N}{\partial y} + g_0\beta\,(T - T_\infty) - \frac{\sigma' B_0^2 u}{\rho_\infty}, \tag{2}$$

$$u\frac{\partial N}{\partial x} + v\frac{\partial N}{\partial y} = \frac{\upsilon_s}{\rho_\infty j}\frac{\partial^2 N}{\partial y^2} - \frac{S}{\rho_\infty j}\left(2N + \frac{\partial u}{\partial y}\right), \tag{3}$$

$$u\frac{\partial T}{\partial x} + v\frac{\partial T}{\partial y} = \frac{k}{\rho_\infty c_p}\frac{\partial^2 T}{\partial y^2} + \frac{Q_0}{\rho_\infty c_p}(T - T_\infty) + \frac{\mu}{c_p\rho_\infty}\left(\frac{\partial u}{\partial y}\right)^2, \tag{4}$$

where u, v are the velocity components along x, y co-ordinates, respectively, μ is the coefficient of dynamic viscosity, S is the microrotation coupling coefficient

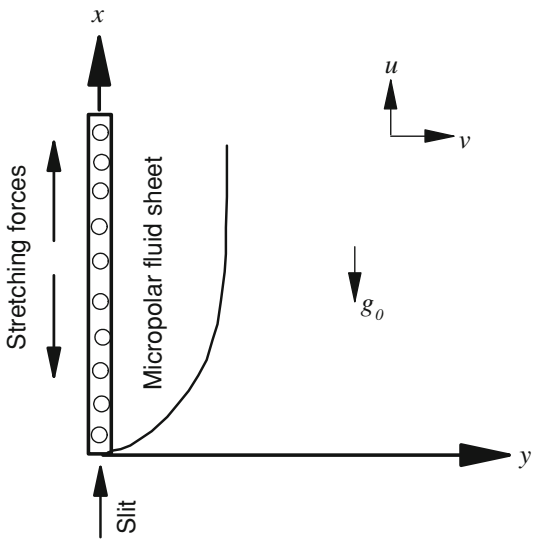

Fig. 1 Flow configurations and coordinate system

(also known as the coefficient of gyro-viscosity or as the vortex viscosity), ρ_∞ is the mass density of the ambient fluid, N is the microrotation component normal to the xy-plane, σ' is the magnetic permeability, $\upsilon_s = (\mu + S/2)j$ is the microrotation viscosity or spin-gradient viscosity, j is the micro-inertia density, T is the temperature of the fluid in the boundary layer, T_∞ is the temperature of the ambient fluid outside the boundary layer, c_p is the specific heat of the fluid at constant pressure, k is the thermal conductivity, and Q_0 is the heat generation or absorption constant.

Boundary conditions of the above problem are

$$\left.\begin{array}{l} u = cx^m, \quad v = \pm\, v_0(x), \quad N = -s\frac{\partial u}{\partial y}, \quad T = T_w (= T_\infty + Ax^p) \text{ at y} = 0, \\ u = 0, \quad N = 0, \quad T = T_\infty \quad \text{as y} \to \infty. \end{array}\right\} \quad (5)$$

Positive and negative values for v_0 indicate blowing and suction, respectively, while $v_0 = 0$ corresponds to an impermeable sheet. In this problem, we have confined our attention to the suction or injection of the fluid through the stretching sheet keeping the suction porosity constant. When the microrotation parameter $s = 0$, we obtain $N = 0$ which represents a no-spin condition, i.e., the microelements in a concentrated particle flow close to the wall are not able to rotate as stated by Jena and Mathur [18]. The case $s = 0.5$ represents vanishing of the anti-symmetric part of the stress tensor and represents weak concentration. For this case Ahmadi [17] suggested that in a fine particle suspension the particle spin is equal to the fluid velocity at the wall. The case corresponding to $s = 1$ is representative of turbulent boundary layer flows.

2.1 Non-dimensionalization

We introduce the following non-dimensional variables:

$$\left.\begin{aligned}\eta = y\sqrt{\frac{c}{\upsilon_\infty}}x^{\frac{m-1}{2}},\ \psi = \sqrt{c\upsilon_\infty x^{m+1}}\ f(\eta),\ N = \sqrt{\frac{c^3}{\upsilon_\infty}}x^{\frac{3m-1}{2}}g(\eta),\ \theta = \frac{T-T_\infty}{T_\mathrm{w}-T_\infty},\end{aligned}\right\} \tag{6}$$

where ψ is the stream function.

Since $u = \frac{\partial\psi}{\partial y}$ and $v = -\frac{\partial\psi}{\partial x}$ we have from Eq. 6,

$$\left.\begin{aligned}u &= cx^m f'(\eta)\\ v &= -\sqrt{c\upsilon_\infty}x^{\frac{m-1}{2}}\left(\tfrac{m+1}{2}f(\eta) + \tfrac{m-1}{2}\eta f'(\eta)\right)\end{aligned}\right\}. \tag{7}$$

Here f is a non-dimensional stream function and the prime symbol denotes differentiation with respect to η.

For a viscous fluid, Ling and Dybbs [44] suggested a temperature-dependent viscosity of the form,

$$\mu = \frac{\mu_\infty}{1+\gamma^*(T-T_\infty)}, \tag{8}$$

where γ^* is the thermal property of the fluid. Equation 8 can be rewritten as

$$\frac{1}{\mu} = B(T-T_\mathrm{r}), \tag{9}$$

where

$$B = \frac{\gamma^*}{\mu_\infty} \quad \text{and} \quad T_\mathrm{r} = T_\infty - \frac{1}{\gamma^*}. \tag{10}$$

In the above Eq. 10, both B and T_r are constants and their values depend on the reference state and γ^*. In general, $B > 0$ for liquids, and $B < 0$ for gases. Typical values of γ^* and B for air are $\gamma^* = 0.026240$ and $B = -123.2$ (see Weast [45]).

The dimensionless temperature θ can also be written as

$$\theta = \frac{T-T_\mathrm{r}}{T_\mathrm{w}-T_\infty} + \theta_\mathrm{r}, \tag{11}$$

where $\theta_\mathrm{r} = \frac{T_\mathrm{r}-T_\infty}{T_\mathrm{w}-T_\infty} = -\frac{1}{\gamma^*(T_\mathrm{w}-T_\infty)} =$ constant, and its value is determined by the viscosity/temperature characteristics of the fluid under consideration and the temperature difference $\Delta T = T_\mathrm{w} - T_\infty$. Using Eq. 11, Eq. 8 becomes

$$\mu = \mu_\infty\left(\frac{\theta_\mathrm{r}}{\theta_\mathrm{r}-\theta}\right). \tag{12}$$

Now substituting Eqs. 6, 7, and 12 into Eqs. 2–4 we obtain the following non-dimensional differential equations,

$$\left(\frac{\theta_r}{\theta_r-\theta}+\Delta\right)f'''+\frac{m+1}{2}ff''-mf'^2+\frac{\theta_r}{(\theta_r-\theta)^2}\theta' f''+\Delta g'-Mf'+\gamma\theta=0 \tag{13}$$

$$\left(\frac{\theta_r}{\theta_r-\theta}+\frac{1}{2}\Delta\right)\xi g''-\Delta\left(2g+f''\right)-\xi\left(\frac{3m-1}{2}f'g-\frac{m+1}{2}g'f\right)=0 \tag{14}$$

$$\theta''+Pr_\infty\left(\frac{m+1}{2}f\theta'-pf'\theta\right)+Pr_\infty Q\theta+Pr_\infty\frac{\theta_r}{\theta_r-\theta}Ecf''^2=0 \tag{15}$$

The dimensionless parameters appeared in Eqs. 13–15 are defined as follows: $\Delta=\frac{S}{\mu_\infty}$ is the vortex viscosity parameter, $M=\frac{\sigma' B_0^2}{\rho_\infty c}x^{1-m}$ is the local magnetic field parameter, $\xi=\frac{jc}{\upsilon_\infty}x^{m-1}$ is the local spin gradient viscosity parameter, $Ec=\frac{(cx^m)^2}{c_p(T_w-T_\infty)}$ is the local Eckert number, $Pr_\infty=\frac{\mu_\infty c_P}{k}$ is the ambient Prandtl number, $Q=\frac{Q_0x^{1-m}}{\rho_\infty c_p c}$ is the local heat source (or sink) parameter, $\gamma=\frac{Gr_x}{Re_x{}^2}$ is the Richardson parameter of which $Gr_x=\frac{g_0\beta(T_w-T_\infty)x^3}{\upsilon_\infty{}^2}$ is the local Grashof number, and $Re_x=\frac{cx^{m+1}}{\upsilon_\infty}$ is the local Reynolds number.

The Prandtl number is a function of viscosity, and as the viscosity varies across the boundary layer, the Prandtl number varies, too. The assumption of a constant Prandtl number inside the boundary layer may produce unrealistic results. Therefore, the Prandtl number related to the variable viscosity is defined by

$$Pr_v=\frac{\mu c_p}{\kappa}=\frac{\left(\frac{\theta_r}{\theta_r-\theta}\right)\mu_\infty c_p}{\kappa}=\left(\frac{\theta_r}{\theta_r-\theta}\right)Pr_\infty. \tag{16}$$

At the surface ($\eta=0$) of the sheet, this can be written as

$$Pr_w=\left(\frac{\theta_r}{\theta_r-1}\right)Pr_\infty. \tag{17}$$

In light of the above discussions, using Eq. 16 the non-dimensional temperature Eq. 15 can be rewritten as

$$\begin{aligned}\theta''\ &+Pr_v\left(1-\frac{\theta}{\theta_r}\right)\left(\frac{m+1}{2}f\theta'-pf'\theta\right)\\&+Pr_vQ\left(1-\frac{\theta}{\theta_r}\right)\theta+Pr_vEcf''^2=0.\end{aligned} \tag{18}$$

From Eq. 16 it can be seen that for large θ_r, i.e., $\theta_r\to\infty$, the variable Prandtl number Pr_v is equal to the ambient Prandtl number Pr_∞, in that case, Eq. 18 reduces to Eq. 15. For $\eta\to\infty$; $\theta(\eta)$ becomes zero; therefore, Pr_v equals Pr_∞ independent

of the values of θ_r. Equation 18 is the corrected non-dimensional form of the energy equation for modeling thermal boundary layer flows with a temperature-dependent viscosity.

The corresponding boundary conditions take the form,

$$\left.\begin{array}{l} f = F_w,\ f' = 1, g = -sf'', \theta = 1 \quad \text{at} \quad \eta = 0, \\ f' = 0,\ \ g = 0,\ \ \theta = 0 \quad \text{as} \quad \eta \to \infty. \end{array}\right\} \tag{19}$$

where $F_w = \pm \frac{v_0(x)}{\sqrt{cv_\infty}\frac{m+1}{2}x^{\frac{m-1}{2}}}$ is the suction or injection parameter. It should be noted that M, ξ, Q, Ec, γ, and F_w are functions of x; therefore, a local similarity approach (Kays and Crawford [46]) is applied to solve the governing Eqs. 13, 14, and 18. Similar studies were made by many authors (see [26], [28–30], [34], Raptis [47], El-Arabawy [48], Aziz [49]) and have been adopted in the present analysis. Therefore, the differential Eqs. 13, 14, and 18 are locally similar. The above-noted systems have been solved numerically for various values of the parameters entering into the problem.

2.2 Local Nusselt Number

The local Nusselt number (or rate of heat transfer) can be defined as

$$Nu_x = -(Re_x)^{\frac{1}{2}}\theta'(0). \tag{20}$$

Thus, from Eq. 20 we see that the local Nusselt number Nu_x is proportional to $-\theta'(0)$. Hence, the numerical values of $Nu_x(Re_x)^{-\frac{1}{2}}$ are calculated from Eq. 20 and are shown in Figs. 8–12. Since the solutions are locally similar, it is to be mentioned that the dimensionless quantity Nu_x is determined locally at any x-station and the upstream history of the flow is ignored, except as it influences the similarity variable.

2.3 Numerical Solutions

The system of non-linear ordinary differential Eqs. 13, 14, and 18 together with the boundary conditions, Eq. 19, are locally similar and solved numerically using the Nachtsheim-Swigert [50] shooting iteration technique (guessing the missing value) along with the sixth-order Runge-Kutta initial value solver.

The boundary conditions, Eq. 19, associated with the non-linear ordinary differential Eqs. 13, 14, and 18 are the two-point asymptotic class, that is, values of the dependent variable are specified at two different values of the independent variable. Specification of an asymptotic boundary condition implies that the first derivative (and higher derivatives of the boundary layer equations, if they exist) of the dependent variable approaches zero as the outer specified value of the independent variable is approached.

For the method of numerically integrating a two-point asymptotic boundary-value problem of the boundary-layer type, the initial-value method is similar to an initial-value problem. Thus, it is necessary to estimate as many boundary conditions at the

surface as were (previously) given at infinity. The governing differential equations are then integrated with these assumed surface boundary conditions. If the required outer boundary condition is satisfied, a solution has been achieved. However, this is not generally the case. Hence, a method must be devised to estimate logically the new surface boundary conditions for the next trial integration. Asymptotic boundary value problems such as those governing the boundary-layer equations are further complicated by the fact that the outer boundary condition is specified at infinity. In the trial integration, infinity is numerically approximated by some large value of the independent variable. There is no a priori general method of estimating these values. Selecting too small a maximum value for the independent variable may not allow the solution to asymptotically converge to the required accuracy. Selecting a large value may result in divergence of the trial integration or in slow convergence of surface boundary conditions. Selecting too large a value of the independent variable is expensive in terms of computer time.

Nachtsheim-Swigert developed an iteration method to overcome these difficulties. In Eq. 19 there are three asymptotic boundary conditions and, hence, three unknown surface conditions such as $f''(0)$, $g'(0)$, and $\theta'(0)$.

Within the context of the initial-value method and the Nachtsheim-Swigert iteration technique, the outer boundary conditions may be functionally represented as

$$Y_j(\eta_{\max}) = Y_j\left(f''(0),\ g'(0),\ \theta'(0)\right) = \delta_j,\ \ j = 1,\ 2\cdots 6, \tag{21}$$

where $Y_1 = f'$, $Y_2 = g$, $Y_3 = \theta$, $Y_4 = f''$, $Y_5 = g'$, and $Y_6 = \theta'$. The last three of these represent asymptotic convergence criteria.

Choosing $f''(0) = y_1$, $g'(0) = y_2$, and $\theta'(0) = y_3$ and expanding in a first-order Taylor series after using Eq. 21 yields

$$Y_j(\eta_{\max}) = Y_{j,C}(\eta_{\max}) + \sum_{i=1}^{3} \frac{\partial Y_j}{\partial y_i}\Delta y_i = \delta_j, \quad j = 1,\ 2\cdots 6 \tag{22}$$

where subscript 'C' indicates the value of the function at $\eta_{\max}$ determined from the trial integration.

Solution of these equations in a least-squares sense requires determination of the minimum value of

$$\text{Error} = \sum_{j=1}^{6} \delta_j^2 \tag{23}$$

with respect to y_i $(i = 1,\ 2,\ 3)$.

Now differentiating Error with respect to y_i, we obtain

$$\sum_{j=1}^{6} \delta_j \frac{\partial \delta_j}{\partial y_i} = 0. \tag{24}$$

Substituting Eq. 22 into Eq. 24 after some algebra, we obtain

$$\sum_{k=1}^{3} a_{ik}\Delta y_k = b_i, \tag{25}$$

where

$$a_{ik} = \sum_{j=1}^{6} \frac{\partial Y_j}{\partial y_i}.\frac{\partial Y_j}{\partial y_k}, \quad b_i = -\sum_{j=1}^{6} Y_{j,C}\frac{\partial Y_j}{\partial y_i}; \quad i,\ k = 1,\ 2,\ 3. \tag{26}$$

Now solving the system of linear Eq. 25 using Cramer's rule, we obtain the missing (unspecified) values of y_i as

$$y_i \cong y_i + \Delta y_i. \tag{27}$$

Thus, adopting the numerical technique aforementioned along with the sixth-order Runge-Kutta initial value solver, the solutions of the non-linear ordinary differential Eqs. 13, 14, and 18 with boundary conditions, Eq. 19, are obtained as a function of the coordinate η for various values of the material parameters.

In all cases a step size of $\Delta\eta = 0.001$ was selected that satisfied a convergence criterion of 10^{-6}. The value of η_∞ was found for each iteration loop by the statement $\eta_\infty = \eta_\infty + \Delta\eta$. The maximum value of η_∞ to each group of the prescribed parameters is determined when the value of the unknown boundary conditions at $\eta = 0$ does not change in the successful loop of iteration with an error of less than 10^{-6}.

With the three different step sizes $\Delta\eta = 0.01$, $\Delta\eta = 0.001$, and $\Delta\eta = 0.005$, we have verified the effects of the step size on the velocity, temperature, and concentration profiles, and in each case, we found excellent agreement among the results. It was found that $\Delta\eta = 0.001$ provided sufficiently accurate results, and further refinement of the grid size was therefore not warranted.

To assess the accuracy of the present code, we compare our quantitative results for a Newtonian fluid along a continuously moving isothermal heated plate with those of Pop et al. [31] and Ali [34] for their zero buoyancy ($\lambda = 0$) case. Thus, setting $\Delta = 0$, $\xi = 0$, $\gamma = 0$, $M = 0$, $Q = 0$, $Ec = 0$, $m = 0$, and $p = 0$ (using the same expression of η defined by [31] and [34] with rescaled current Eqs. 13 and 18 to be consistent), we have calculated values of $f''(0)$ and $\theta'(0)$. For the shake of comparison and to be consistent with [31] and [34] (where the Prandtl number is considered as constant), we also considered the Prandtl number as a constant within the boundary layer. Tables 1 and 2 demonstrate the comparison of the data produced by the present code and those of Pop et al. [31] and Ali [34]. In fact, the results show close agreement, and hence justify the use of the present code.

Table 1 Comparisons of $f''(0)$ to previously published data at $Pr_\infty = 0.7$ and $\Delta = 0$, $\xi = 0$, $\gamma = 0$, $M = 0$, $Q = 0$, $Ec = 0$, $m = 0$, $p = 0$ for different values of θ_r using the same expression of $\eta = \frac{y}{x} Re^{1/2}$ defined by [31] and [34] with rescaled Eqs. 13 and 18 to be consistent

θ_r	Pop et al. [31]	Ali [34]	Present results
−8.0	−0.4773578	−0.4763230	−0.4763475
−0.1	−1.5061732	−1.4965150	−1.4965351
−0.01	−4.4856641	−4.4683560	−4.4577559
8.0	−0.4089153	−0.4083475	−0.4083562

Table 2 Comparisons of $\theta'(0)$ as in Table 1

θ_r	Pop et al. [31]	Ali [34]	Present result
−8.0	−0.3493189	−0.3432339	−0.3436723
−0.1	−0.2191391	−0.1652394	−0.1661476
−0.01	−0.1544918	−0.0561845	−0.0764055
8.0	−0.3605226	−0.3555822	−0.3560031

3 Numerical Results and Discussion

For the purpose of discussing the results, the numerical calculations are presented in the form of non-dimensional temperature profiles. In the calculations the values of the parameters, namely, the Richardson parameter γ, variable Prandtl number Pr_v, viscosity parameter θ_r, magnetic field parameter M, heat source (or sink) parameter Q, Eckert numberEc, suction (or injection) parameter F_w, stretching index m, and temperature index p are varied. The choice of the values of the parameters was dictated by the values chosen by previous investigators. Because of the lack of experimental data for the vortex viscosity parameter Δ, the micro-inertia density parameter ξ, and the microrotation parameter s, suitable representative values are chosen in order to determine the polar effects on the flow characteristics. When viscosity does not depend on the temperature values of the ambient Prandtl number, $Pr_\infty = 0.73$, 2.97, and 7 correspond to air, methyl chloride, and water. When the viscosity depends on the temperature these values at the surface of the sheet ($\eta = 0$) and for $\theta_r = 2$ correspond to 1.46, 5.94, and 14. Therefore, in the simulation the values of the variable Prandtl number are chosen as 1.46, 5.94, and 14. Since $\gamma = \frac{Gr_x}{Re_x{}^2}$ represents the ratio of the buoyancy forces to the inertial forces, $\gamma = 1$ corresponds to mixed convection, $\gamma \ll 1$ corresponds to forced convection, and $\gamma \gg 1$ corresponds to free convection. Physically $\gamma < 0$ corresponds to an externally heated sheet and $\gamma > 0$ corresponds to an externally cooled sheet while $\gamma = 0$ corresponds to the absence of free convection currents. Since the free convection problem is considered, only a positive large value of γ is considered. The default values of the parameters are chosen as $\gamma = 10$, $Pr_v = 1.46$, $\theta_r = 2$, $M = 1$, $Q = 0.5$, $Ec = 0.2$, $m = 1.5$, $p = 1.5$, $\Delta = 0.5$, $\xi = 1$, and $s = 0.5$, unless otherwise stated.

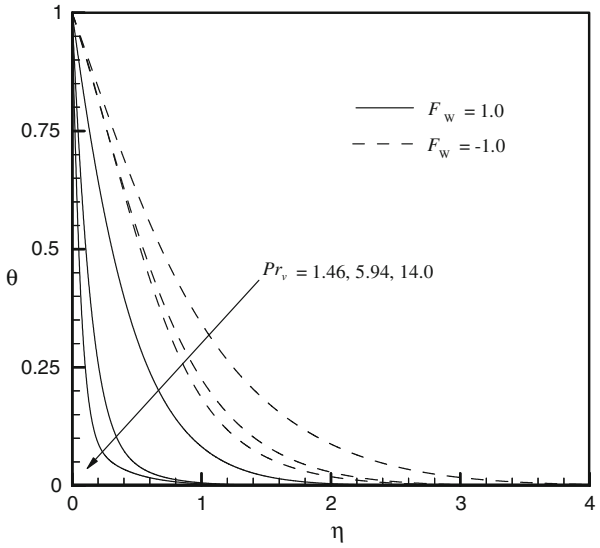

Fig. 2 Dimensionless temperature profiles for different values of Pr_v

Figure 2 shows the temperature profiles for different values of the variable Prandtl number Pr_v for a cooled surface for both cases of fluid suction and injection. As the Prandtl number increases, viscous forces tend to suppress the buoyancy forces and cause the temperature in the thermal boundary layer to decrease. It is also noticeable that for a fixed value of the Prandtl number, the temperature corresponding to the case of fluid suction is lower compared to the case of fluid injection. That is, the thickness of the thermal boundary layer is higher for fluid injection than for fluid suction.

In Fig. 3 we have varied the viscosity parameter (θ_r) keeping the values of all other parameters fixed. Figure 3 reveals that the temperature profile as well as the thickness of the thermal boundary layer decrease when θ_r increases for both cases of fluid suction and injection.

Figure 4 explains the variation of the heat generation (or absorption) parameter (Q) on the temperature profiles. Because of the presence of heat generation, it is apparent from this figure that there is an increase in the thermal state of the fluid; as a consequence, we observe that temperature profiles increase as Q increases for both cases of fluid suction and injection. But the opposite effect is observed for the case of heat absorption. The thickness of the thermal boundary layer is higher for fluid injection than for fluid suction for both cases of heat generation or absorption.

Figure 5 illustrates the dimensionless temperature profiles for different values of the viscous dissipation parameter (or Eckert number) Ec. From this figure it can be seen that temperature profiles have an increasing effect for increasing values of Ec. Therefore, increasing the Eckert number broadens the thickness of the thermal boundary layers.

Figure 6 depicts the effects of the stretching index (m) on the temperature profiles. It is found from Fig. 6 that temperature profiles decrease quite rapidly with an increase

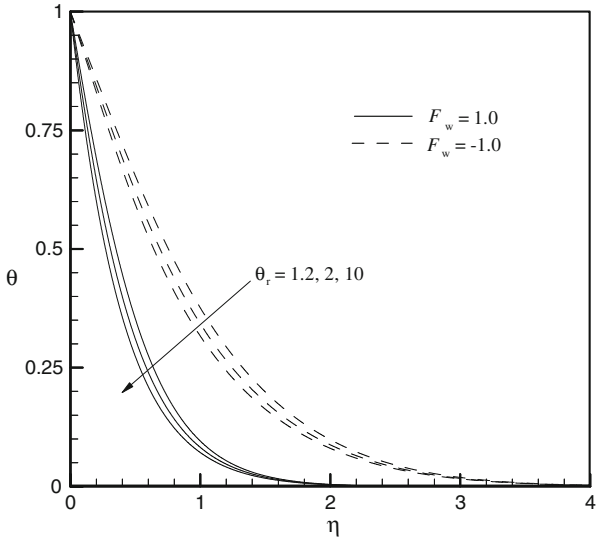

Fig. 3 Dimensionless temperature profiles for different values of θ_r

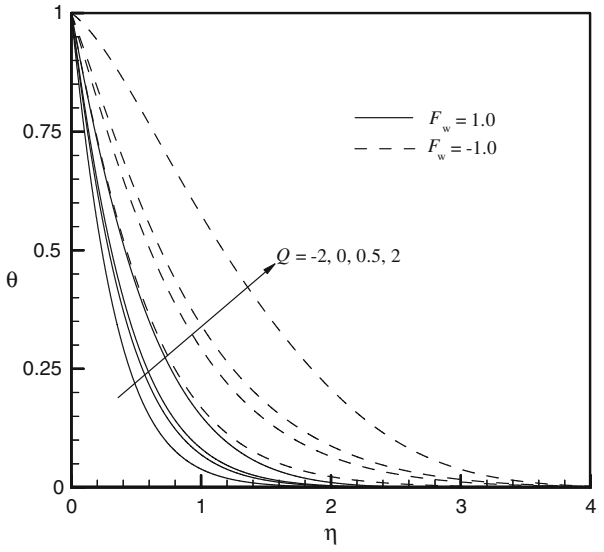

Fig. 4 Dimensionless temperature profiles for different values of Q

of m for the case of fluid suction while it increases for the case of fluid injection. It is also noticeable that for fluid injection temperature profiles crossover away from the surface of the plate and decrease with an increase of m. The value $m = 0$ represents a uniformly moving surface. From this figure we also find that heat transfer in a uniformly moving surface is higher than in a stretched surface.

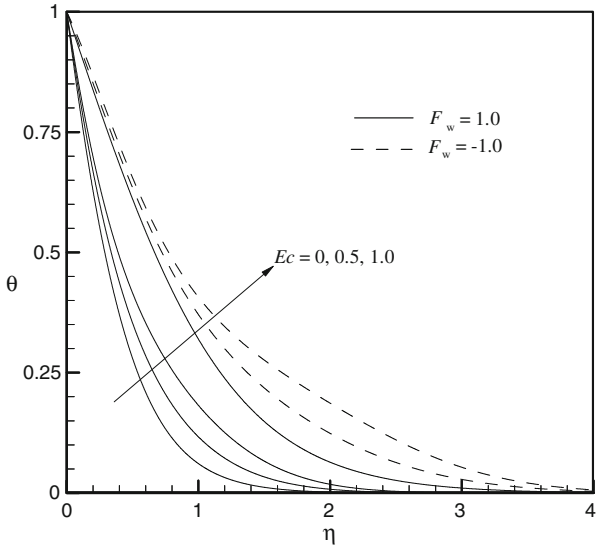

Fig. 5 Dimensionless temperature profiles for different values of Ec

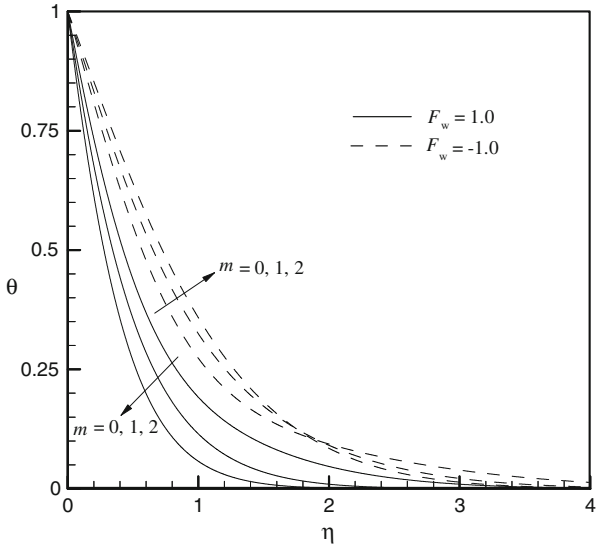

Fig. 6 Dimensionless temperature profiles for different values of m

Figure 7 presents the variation of the temperature index (p) on the temperature profiles. From here we see that temperature profiles decrease very rapidly in the case of fluid injection compared to the case of fluid suction with the increase of p. The value $p = 0$ represents a uniformly heated surface. Figure 7 also shows that the temperature in a uniformly heated surface is higher than in a variably heated surface.

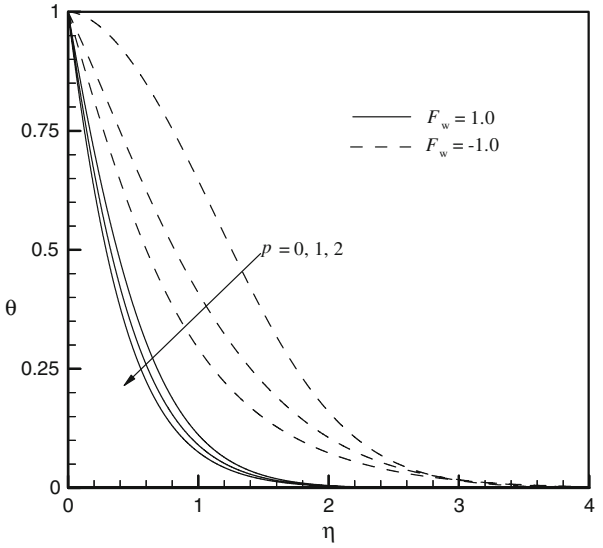

Fig. 7 Dimensionless temperature profiles for different values of p

Figure 8 shows the local rate of heat transfer ($Nu_x Re_x^{-1/2}$) for different values of the Richardson parameter γ and Prandtl number Pr_v. This figure reveals that for a fixed Prandtl number value the local heat transfer coefficient increases with the increase of the Richardson parameter for both cases of fluid suction and injection. On the other hand, values of $Nu_x Re_x^{-1/2}$ increase very rapidly with the increase of the Prandtl number for the case of fluid suction compared to that of fluid injection. Thus, applying suction and (or) injection, one can significantly control the heat transfer from the heated surface to the fluid.

Figures 9 and 10 show the variation of $Nu_x Re_x^{-1/2}$ for different values of heat generation (or absorption) parameter Q and viscosity parameter θ_r. From these figures we found that for a fixed value of the viscosity parameter the local rate of heat transfer from the surface to the fluid decreases with the increase of the heat generation parameter for both fluid suction and injection. This is due to the fact that as heat is generated, the thermal state of the surrounding fluid increases; as a consequence, the rate of heat transfer from the surface to the fluid decreases. The opposite trend is observed for the case of heat absorption. The increase in $Nu_x Re_x^{-1/2}$ is quite significant for the case of heat generation compared to that for heat absorption. Figure 9 shows that for a positive value of $\theta_r = 2$, $Nu_x Re_x^{-1/2}$ decreases by approximately 33.5 % in the case of fluid suction while the corresponding decrease is approximately 79 % for the case of fluid injection when Q increases from 0 to 2. Whereas Fig. 10 reveals that for a negative value of $\theta_r = -2$, $Nu_x Re_x^{-1/2}$ decreases by approximately 32.4 % in the case of fluid suction while the corresponding decrease is approximately 96.5 % for the case of fluid injection when Q increases from 0 to 2. These figures also show that values of $Nu_x Re_x^{-1/2}$ increase with the increase of the viscosity parameter θ_r for both fluid suction and injection. At the instant of $Q = 2$, the value of $Nu_x Re_x^{-1/2}$ increases

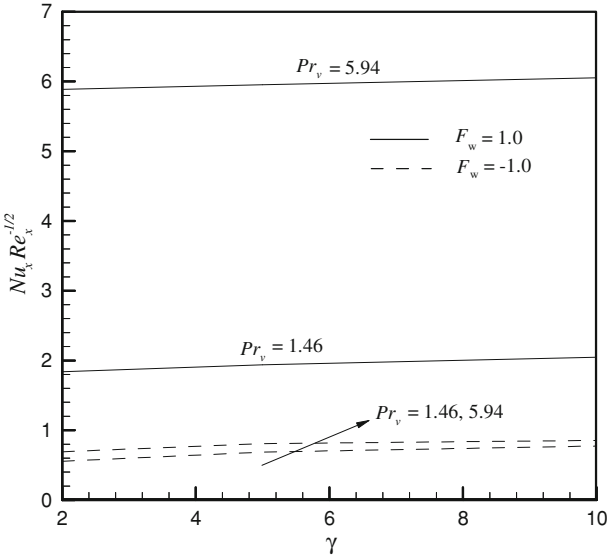

Fig. 8 Local Nusselt number for different values of γ and Pr_v

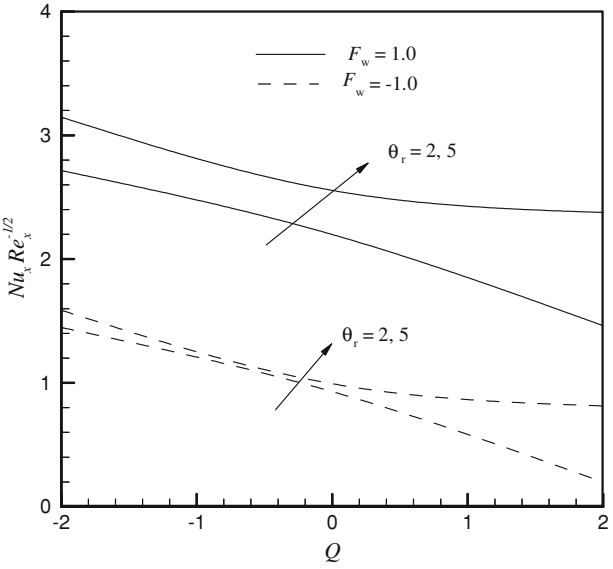

Fig. 9 Local Nusselt number for different values of Q and $\theta_r > 0$

by approximately 62.6 % for the case of fluid suction while it increases by 312.4 % for the case of fluid injection when the values of θ_r increase from 2 to 5. These figures also reveal that when θ_r is positive; the increasing effect of θ_r (>0) on $Nu_x Re_x^{-1/2}$ is quite significant compared to θ_r (<0) for the case of heat generation. The opposite effect is observed for the case of heat absorption.

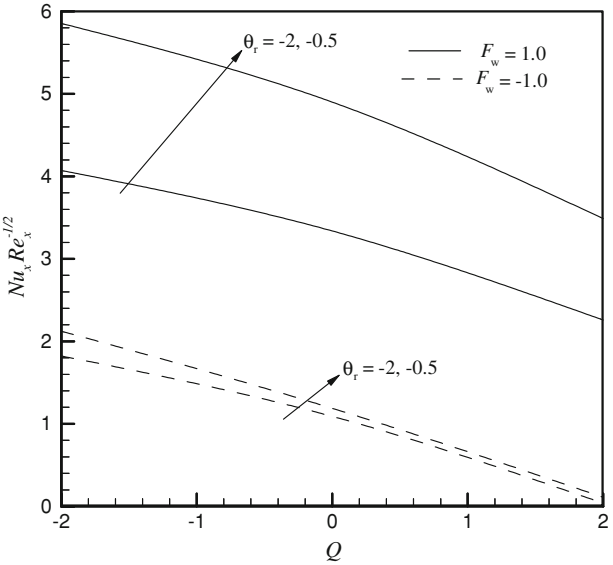

Fig. 10 Local Nusselt number for different values of Q and $\theta_r < 0$

Figure 11 presents the variation of $Nu_x Re_x^{-1/2}$ for different values of the Eckert number and the magnetic field parameter for both cases of fluid suction and injection. From here we found that for a fixed value of M, the local Nusselt number $Nu_x Re_x^{-1/2}$decreases with the increase of Ec for both cases of fluid suction and injection. This figure also reveals that the local Nusselt number decreases with the increase of M for all values of Ec in the case of fluid suction, while for the case of fluid injection, the local Nusselt number decreases for $Ec < 0.4$ (not precisely determined). Outside this range of Ec, the local Nusselt number increases with the increase of M for fluid injection.

Figure 12 shows the local Nusselt number for various values of the stretching index m and temperature index p for both the cases of fluid suction and injection. From here we found that the value of $Nu_x Re_x^{-1/2}$ increases with the increase of the velocity index as well as the temperature index for fluid suction. The opposite trend is observed for the case of fluid injection.

Figure 13 depicts the variable Prandtl number within the boundary layer for various values of the viscosity parameter θ_r at an ambient Prandtl number $Pr_\infty = 0.73$. From this figure we see that Pr_v asymptotically converges to the value of Pr_∞ as $\eta \to \infty$. It is also notable that at the surface of the sheet Pr_v approaches Pr_∞ for large values of θ_r. For $\theta_r > 0$; Pr_v decreases with the increase of θ_r while an opposite effect is observed for $\theta_r < 0$.

In Table 3 we have presented the local Nusselt number for various values of the viscosity parameter θ_r while considering the Prandtl number to be constant (using energy Eq. 15) and variable (using energy Eq. 18) within the boundary layer. Since the viscosity is a function of the temperature, so is the Prandtl number. For $\theta_r \in (0, 1]$, no solutions can be found. From this table it is clear that for very large values of θ_r

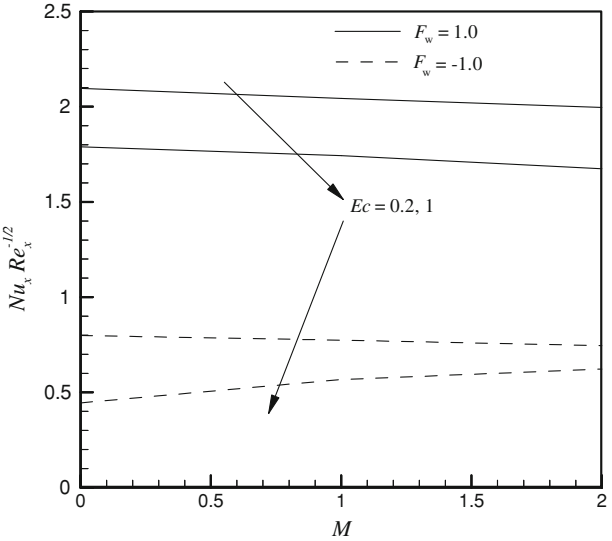

Fig. 11 Local Nusselt number for different values of M and Ec

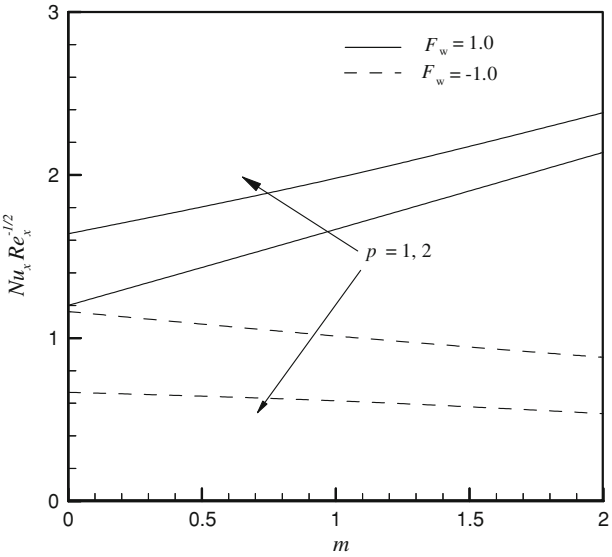

Fig. 12 Local Nusselt number for different values of m and p

(whether positive or negative), absolute errors between the produced results differ by less than 1 %. For $\theta_r \to 1^+$, the absolute error between the results is markedly large, but for negative values of $\theta_r \to 0^-$, the absolute error between the results becomes enormously large. At $\theta_r = 1.001$ the absolute error between the results is more than 72 %, whereas for $\theta_r = -0.05$, this becomes more than 580 %. These results produce clear evidence for modeling thermal boundary layer flow with a temperature-depen-

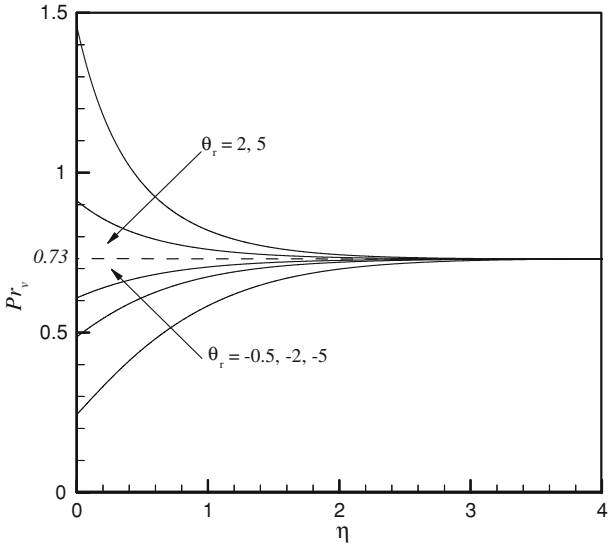

Fig. 13 Variable Prandtl number versus η for different values of θ_r

Table 3 Values of $Nu_x Re_x^{-1/2}$ for different values of θ_r

θ_r	$Nu_x Re_x^{-1/2}$		Absolute error $= \left\vert \frac{\text{i}-\text{ii}}{\text{i}} \right\vert \times 100$
	(i) For constant Prandtl number	(ii) For variable Prandtl number	
−100.0	1.605300	1.611378	< 1
−10.0	1.606471	1.666908	3.76
−2.0	1.611352	1.906984	18.35
−0.5	1.625711	2.743549	68.76
−0.1	1.657920	6.686586	303.31
−0.05	1.670647	11.361811	580.10
1.001	1.590837	0.922775	72.40
1.01	1.590960	0.929753	41.56
1.2	1.593224	1.048450	34.19
2	1.598177	1.282450	19.76
10	1.603833	1.542617	3.82
100	1.605036	1.598951	< 1
∞	1.605168	1.605168	0

dent viscosity while considering the Prandtl number as a constant within the boundary layer may produce unrealistic results. In Table 3, $\theta_r \to \infty$ indicates that the viscosity is independent of temperature, i.e., constant. Thus, the local rate of heat transfer in a fluid of constant viscosity is higher than in a fluid of variable viscosity when θ_r is positive. An opposite result is found for negative values of θ_r.

4 Conclusions

In this paper, the problem of steady, laminar, hydromagnetic free convection flow of a micropolar fluid past a non-linear stretching sheet with variable viscosity and variable wall temperature in the presence of heat generation (or) absorption is studied numerically. Using similarity transformations the governing equations of the problem have been transformed into non-linear ordinary differential equations and solved for local similar solutions by using the Nachtsheim-Swigert shooting iteration technique. From the present study the following conclusions can be drawn:

1. The local rate of heat transfer ($Nu_x Re_x^{-1/2}$) increases with an increase of the Richardson parameter γ, variable Prandtl number Pr_v, viscosity parameter θ_r, whereas it decreases with an increase of the heat generation parameter Q and Eckert number Ec for both the cases of fluid suction and injection.
2. The local rate of heat transfer increases with the increase of the stretching index m and temperature index p for the case of suction. An opposite effect is observed for the case of fluid injection.
3. The local rate of heat transfer decreases with the increase of the magnetic field parameter M for the case of fluid suction. But for the case of fluid injection, $Nu_x Re_x^{-1/2}$ decreases with the increase of M for $Ec < 0.4$, and beyond this value of Ec, $Nu_x Re_x^{-1/2}$ increases with the increase of M.
4. The absolute error in the Nusselt number is enormously large for lower negative values of the viscosity parameter θ_r if the Prandtl number is considered as a constant rather than a variable inside the boundary layer.
5. For modeling thermal boundary layers with a temperature-dependent viscosity, the Prandtl number must be treated as a variable inside the boundary layer.
6. The local rate of heat transfer in a fluid of constant viscosity is higher than that in a fluid of a temperature-dependent viscosity when θ_r is positive, whereas an opposite result is found for $\theta_r < 0$.

References

1. B.C. Sakiadis, AIChE J. **7**, 26 (1961)
2. L.E. Erickson, L.T. Fan, V.G. Fox, Ind. Eng. Chem. Fund. **5**, 19 (1966)
3. F.K. Tsou, E.M. Sparrow, R.J. Goldstien, Int. J. Heat Mass Transfer **10**, 219 (1967)
4. P.S. Gupta, A.S. Gupta, Can. J. Chem. Eng. **55**, 744 (1977)
5. A. Chakrabarti, A.S. Gupta, Quart. Appl. Math. **3**, 73 (1979)
6. T.C. Chiam, Int. J. Eng. Sci. **33**, 429 (1995)
7. P. Chandran, N.C. Sacheti, A.K. Singh, Int. Commun. Heat Mass Transfer **23**, 889 (1996)
8. K. Vajravelu, A. Hadjinicalaou, Int. J. Eng. Sci. **35**, 1237 (1997)
9. C.K. Chen, N.I. Char, J. Math. Anal. Appl. **135**, 568 (1988)
10. M.E. Ali, Int. J. Heat Fluid Flow **16**, 280 (1995)
11. C.-H. Chen, Int. J. Therm. Sci. **47**, 954 (2008)
12. R. Cortell, Appl. Math. Comput. **184**, 864 (2007)
13. R. Cortell, Phys. Lett. A **372**, 631 (2008)
14. R. Cortell, J. Mater. Process. Tech. **203**, 176 (2008)
15. A.C. Eringen, J. Math. Mech. **16**, 1 (1966)
16. A.C. Eringen, J. Math. Anal. Appl. **38**, 480 (1972)
17. G. Ahmadi, Int. J. Eng. Sci. **14**, 639 (1976)

18. S.K. Jena, M.N. Mathur, Int. J. Eng. Sci. **19**, 1431 (1981)
19. R.S.R. Gorla, H.S. Takhar, Int. J. Eng. Sci. **25**, 949 (1987)
20. R.S.R. Gorla, Int. J. Eng. Sci. **26**, 385 (1988)
21. A. Yucel, Int. J. Eng. Sci. **27**, 1593 (1989)
22. R.S.R. Gorla, P.P. Lin, A.J. Yang, Int. J. Eng. Sci. **28**, 525 (1990)
23. R.S.R. Gorla, Int. J. Eng. Sci. **30**, 349 (1992)
24. M.A. Hossain, M.K. Chaudhury, Acta Mech. **131**, 139 (1998)
25. D.A.S. Rees, I. Pop, IMAJ Appl. Math. **61**, 179 (1998)
26. M.M. Rahman, M.A. Sattar, ASME J. Heat Transfer **128**, 142 (2006)
27. M.M. Rahman, M.A. Sattar, Int. J. Appl. Mech. Eng. **12**, 497 (2007)
28. M.M. Rahman, T. Sultana, Nonlinear Anal. Model. Control **13**, 71 (2008)
29. M.M. Rahman, Commun. Nonlinear Sci. Numer. Sim. **14**, 3018 (2009)
30. M.M. Rahman, I.A. Eltayeb, S.M.M. Rahman, Therm. Sci. **13**, 23 (2009)
31. I. Pop, R.S.R. Gorla, M. Rashidi, Int. J. Eng. Sci. **30**, 1 (1992)
32. E.M.A. Elbashbeshy, M.A.A. Bazid, J. Phys. D. Appl. Phys. **33**, 2716 (2000)
33. M.S. Abel, S.K. Khan, K.V. Prasad, Int. J. Non-Linear Mech. **37**, 81 (2002)
34. M.E. Ali, Int. J. Therm. Sci. **45**, 60 (2006)
35. A. Pantokratoras, Int. J. Heat Mass Transfer **45**, 963 (2002)
36. A. Pantokratoras, Int. J. Eng. Sci. **42**, 1891 (2004)
37. S. Mukhopadhyay, G.C. Layek, Sk.A. Samad, Int. J. Heat Mass Transfer **48**, 4460 (2005)
38. M.S. Alam, M.M. Rahman, M.A. Samad, Nonlinear Anal. Model. Control **14**, 3 (2009)
39. M.M. Rahman, K.M. Salahuddin, Commun. Nonlinear Sci. Numer. Sim. (2009) doi:10.1016/j.cnsns.2009.08.012
40. A.A. Mohammadein, R.S.R. Gorla, Int. J. Numer. Meth. Heat Fluid Flow **11**, 50 (2001)
41. A. Desseaux, N.A. Kelson, ANZIAM J. **42**(E), C536 (2000)
42. R. Bhargava, S. Sharma, H.S. Takhar, O.A. Beg, P. Bhargava, Nonlinear Anal. Model. Control **12**, 45 (2007)
43. T. Hayat, Z. Abbas, T. Javed, Phys. Lett. A **372**, 637 (2008)
44. J.X.Ling, A. Dybbs, ASME Paper 87-WA/HT-23 (New York, 1987)
45. R.C. Weast, *CRC Handbook of Chemistry and Physics*, 71st edn. (CRC Press, Boca Raton, Florida, 1990)
46. W.M. Kays, M.E. Crawford, *Convective Heat and Mass Transfer*, 2nd edn. (McGraw-Hill, New York, 1987)
47. A. Raptis, Int. J. Heat Mass Transfer **41**, 2865 (1998)
48. H.A.M. El-Arabawy, Int. J. Heat Mass Transfer **46**, 1471 (2003)
49. A. Aziz, Commun. Nonlinear. Sci. Numer. Sim. **14**, 1064 (2009)
50. P.R. Nachtsheim, P. Swigert, *Satisfaction of the asymptotic boundary conditions in numerical solution of the system of non-linear equations of boundary layer type* (NASA TND-3004, 1965)